ARTICLES

Different Real and Imaginary Components of the Resonant Third-Order Polarization Revealed by Optical Heterodyne Detected Transient Grating Spectroscopic Studies of Crystal Violet: Model and Experiment†

Qing-Hua Xu, Ying-Zhong Ma, and Graham R. Fleming*

Department of Chemistry, University of California, Berkeley and Physical Biosciences Division, Lawrence Berkeley National Laboratory, Berkeley, California 94720

Received: December 31, 2001; In Final Form: June 14, 2002

We carried out heterodyne detected transient grating measurements on a triphenylmethane (TPM) dye molecule, crystal violet, in ethanol, to investigate the origin of the apparently contradictory wavelength dependence observed in pump−probe and homodyne detected transient grating experiments. The measurements were performed at two different wavelengths and the decay profiles of the real and imaginary components of the third-order polarization were found to be strikingly different at both wavelengths. A simple model that accounts for the additional contribution from hot ground state absorption is proposed. The model successfully explains the major features observed in the experiments and provides a consistent picture for the underlying dynamics in this type of system. The striking differences between the decay profiles and wavelength dependencies of the real and imaginary components of $P^{(3)}$ observed in the TPM molecules predominantly originate from the different wavelength dependence of the amplitudes of the various contributions, rather than from changes in the time scales or the observation of new contributions at particular wavelengths.

I. Introduction

The rapid developments in ultrashort laser pulse generation[1,2] have allowed ultrafast four-wave mixing (FWM) spectroscopy[1−5] to be widely applied to the study of photophysical and photochemical processes in the condensed phase. Pump−probe (PP) and transient grating (TG) are two closely related FWM techniques, and both are mainly sensitive to the population dynamics and the spectral diffusion process.[5] PP is probably the simplest and most widely used FWM technique, and the intrinsic heterodyne nature of its detection scheme makes it a useful tool for detecting very weak signals. However, it is only sensitive to the imaginary component of the third-order polarization $P^{(3)}$ (i.e., transient absorption component). Many physical and chemical processes, such as thermal grating, will contribute solely to the real component of $P^{(3)}$ (i.e., transient dispersion component, the so-called phase grating), which can be probed by the TG technique.[4−7] Conventional TG measurements are usually performed in a homodyne manner and the signal is proportional to the modulus squared of the third-order polarization $P^{(3)}$, i.e., sum squared of the real and imaginary components.

In simple systems, the acoustic thermal grating can be ignored when the probe wavelength falls in a strong absorption band,[8] especially if low repetition rate laser sources are used. It has been demonstrated by Joo et al.[9] that, in the absence of an acoustic grating, TG and PP measure the same dynamics in simple two-level systems, which implies that the electronic contribution to the real and imaginary components of $P^{(3)}$ reflect the same dynamics. This was confirmed by our recent heterodyne TG studies in a simple resonant system, rhodamine 640 dissolved in dimethyl sulfoxide (DMSO).[10] The real and imaginary components in the longer population time region (>200 fs) were found to exhibit the same decay behavior, although the amplitude of the real component is strongly dependent on the excitation wavelength and changes sign on the two sides of the absorption spectrum. In these studies, the initial portion of the real response was found to be contaminated by the interference with the nonresonant solvent contribution.

Even though the electronic contribution to the real and imaginary components of $P^{(3)}$ in nonresonant liquids is well-known to be different,[11−13] little attention has been paid to the possible different electronic contributions to the real and imaginary components in resonant systems.[14,15] Our previous study of the isomerization of 1,1′-diethyl-4,4′-cyanine (1144C) with different FWM techniques[15] showed strikingly different wavelength dependence in the decay behavior for the PP and homodyne TG signals, suggesting that different decay profiles can be associated with the real and imaginary components of the $P^{(3)}$. Similar differences in the wavelength dependence of PP and homodyne TG signals were also observed in crystal violet and malachite green,[16] leading us to suspect that such differences are a common feature of systems with ultrafast decay to the ground state. To determine the origin of the different PP and TG profiles, separate measurements of the real and imaginary components of third-order polarization $P^{(3)}$ using optical heterodyne detection are necessary.

Rather few studies have been carried out using heterodyne detection for third-order resonant signals probably because of the lack of a reliable and simple heterodyne detection technique

† Part of the spcial issue "R. Stephen Berry Festschrift".

10.1021/jp014714n CCC: $22.00
Published on Web 08/28/2002

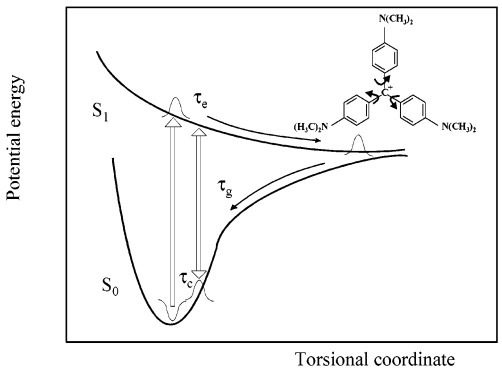

Figure 1. Schematic potential energy surfaces and molecular structure for crystal violet.

that can provide the arbitrary phase control necessary to measure both the real and imaginary components of $P^{(3)}$. Conventional methods for heterodyne detection via an active phase-locking technique using an interferometer[17−19] are limited by their experimental complexity and limited phase stability. A novel optical heterodyne detected transient grating (OHD-TG) technique based on diffractive optics was introduced by Miller and co-workers[20−23] and Nelson and co-workers[24] and has been shown to be a straightforward and reliable method of providing full access to the advantages of the heterodyne detection method. To remove contamination from the pump−probe signal in the same phase-matching direction of the TG signal, Tokmakoff et al.[25] introduced a dual diffractive optics method. Recently, we made some modifications to the arrangement used by Miller et al.[20−23] to produce a simple OHD-TG method with a single diffractive optical element.[26] The technique features ease of alignment, is free of PP contamination, and suppresses scattering of the input beams. In this work, we used this method to perform OHD-TG measurements on two typical triphenylmethane (TPM) molecules, crystal violet (CV) and malachite green (MG).

The excited-state dynamics of the triphenylmethane (TPM) dyes have long been studied as a prototype for solution-phase chemical reactions involving large-amplitude motion.[27−30] Their excited states are much shorter-lived than that of a typical fluorescent dye molecule.[31,32] The fluorescence lifetimes, quantum yields, and ground state recovery dynamics of the TPM molecules have been found to be strongly dependent on the solvent viscosity.[31] The excited state dynamics of the TPM molecules is usually described by reference to the schematic potential energy surfaces shown in Figure 1a. Upon excitation, the molecule will propagate toward the energy minimum between the S_1 and S_0 states, where a nonadiabatic transition occurs to bring the population down to the ground-state surface followed by the further relaxation to the original ground state. The propagation on S_1 and S_0 is associated with a continuous large amplitude torsional motion of the three phenyl rings.[31] Different theoretical models[28−30] have been proposed to explain the excited-state relaxation process in the TPM molecules. The model proposed by Bagchi, Fleming, and Oxtoby (BFO)[30] has been successful in explaining many of the qualitative features of the experimental observations such as the fractional viscosity dependence of the fluorescence quantum yield, the viscosity dependence of excited-state lifetimes, the turnover of the activation energy with viscosity change, and the initial delay before the ground-state recovery (the induction period). A quantitative understanding of the barrierless motion, nonadiabatic transition, and vibrational redistribution and cooling processes requires, inter alia, accurate characterization of the time scales of the various phases of the overall process. This has been hampered by ambiguity in interpreting conventional spectroscopic signals and by apparently contradictory behavior when the same process is observed by different third-order optical techniques.[15] The present work is aimed at providing a consistent interpretation of the third-order nonlinear spectroscopy of crystal violet, which we hope will provide a basis for descriptions of the spectroscopic observations that incorporate detailed descriptions of the nuclear and electronic relaxation in these prototypical molecules. The measurements were performed on two typical TPM molecules, CV and MG, and because of the close similarity of the results, only the data for CV are presented here. The data reveal strikingly different wavelength dependence in the decay profiles of the real and imaginary components of $P^{(3)}$. This difference was found to be responsible for the apparently contradictory results obtained from PP and homodyne TG measurements. To understand the origin of this difference, we propose a simple model that includes a contribution from hot ground-state absorption and the calculations based on this model are able to reproduce the major decay features observed experimentally.

II. Experimental Section

The OHD-TG was performed by using a simplified diffractive optics (DO) based arrangement as described previously.[26] Briefly, the pulse generated from a regenerative Ti:sapphire amplifier pumped optical parametric amplifier (OPA) with a repetition rate of 250 kHz was compressed to ∼40 fs with a prism pair and split into a strong pump and a weak probe beam with an intensity ratio of ∼10:1, and the maximal pulse energy of the pump beam was ∼1.3 nJ at the sample position. The two beams were spatially overlapped on a DO (Rochester Photonics) with a quartz lens of 20-cm focal length. Each of the two beams was split into two replicas (±1 diffractive orders) with an efficiency of ∼30% and the crossing angle between two replicas was set to ∼2°. The resulting four beams were achromatically imaged onto the sample by a combination of an Al-coated concave spherical mirror with a 50-cm radius and a fold mirror. The spherical mirror was placed one radius away from the DO and was slightly tilted off-axis horizontally to separate the outgoing beams from the incoming beams. Following the phase-matching geometry, the signal ($\mathbf{k}_s = \mathbf{k}_1 - \mathbf{k}_2 + \mathbf{k}_3$) was radiated along the $\mathbf{k}_4$ direction ($\mathbf{k}_4$ acts as local oscillator, LO) and thus was heterodyne detected. The probe beam ($\mathbf{k}_3$) was chopped at 1150 Hz right in front of the sample, and the signal was detected with a silicon photodiode and a lock-in amplifier. A 150-μm-thick microscope cover slip was inserted into the probe ($\mathbf{k}_3$) and LO ($\mathbf{k}_4$) paths. The cover slip in the LO path was mounted on a rotating stage whose fine adjustment allows control of the phase difference between the LO and signal fields.

The PP measurements were carried out with the same setup, with beams $\mathbf{k}_1$ and $\mathbf{k}_3$ blocked and with the pump beam chopped in front of the DO. The homodyne TG signal can also be recorded with the same setup by blocking the fourth beam ($\mathbf{k}_4$, LO). However, since the homodyne signal recorded by using this experimental arrangement is very weak and could easily be contaminated by the scattering from the other beams and therefore become partially heterodyned,[19,26] the homodyne TG signal presented here was measured in an equilateral triangle geometry with equal intensities of the three incoming beams as previously described.[15,33] In all the experiments, the polarization of the all the beams is kept parallel. The reorientation relaxation effect can be ignored, since the lifetime here is much shorter than the corresponding reorientation time.

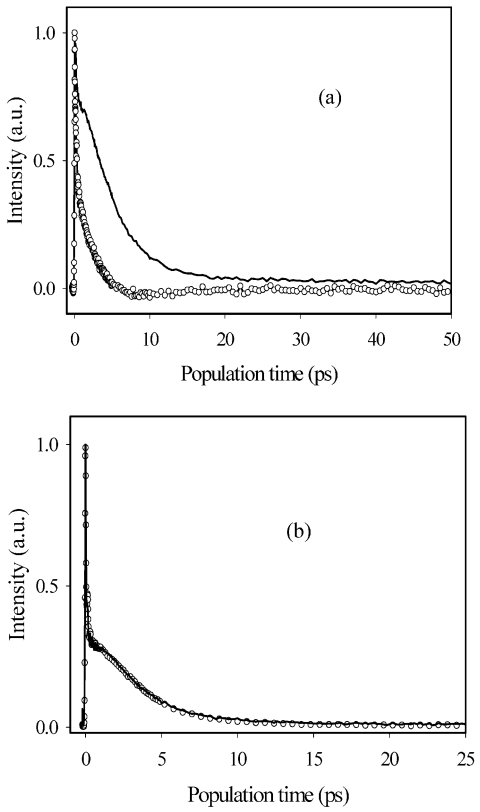

Figure 2. (a) Pump−probe and (b) homodyne TG profiles for crystal violet in ethanol measured at 593 nm (solid lines) and 620 nm (symbols).

Crystal violet (CV), ethanol, and carbon disulfide (CS_2) were purchased from Aldrich and were used as received. The absorption spectrum (Figure 1b) was measured using a Shimadzu UV−visible spectrometer. A glass flow sample cell with 1 mm path length was used for the measurements on CV/ethanol and the solution was circulated by using a gear pump, to avoid any possible thermal heating effect. The concentration of dye molecules was adjusted to give an OD of 0.8 per mm at the corresponding excitation wavelength in the measurements.

III. Results

III.A. Pump−Probe (PP) and Homodyne Transient Grating (TG) Measurements. The PP and homodyne TG measurements for CV in ethanol were performed at 593 and 620 nm and the decay profiles are shown in Figure 2. These two wavelengths are located, respectively, at the peak position and the red edge of the absorption spectrum. It can be seen that the profiles of the PP and TG signals exhibit strikingly different wavelength dependence. As the wavelength is shifted to the red, the PP signal decay becomes considerably faster. At 620 nm, the PP signal rapidly decays to zero, changes sign, and finally recovers back to zero at longer times. However, the TG decay profiles at the two wavelengths are almost identical. TG measurements over a much broader wavelength range show that the decay of the TG becomes only slightly faster as the wavelength is shifted to the blue (data not shown), which is in contrast to the wavelength dependence of the PP signal. This striking difference in the wavelength dependence between the two measurements indicates that the homodyne TG signal cannot be simply understood as the square of the corresponding PP signal, which would be the case if the real and imaginary components of $P^{(3)}$ decayed in an identical manner or no real component is present.

The wavelength dependence of the PP decays observed in the present work is consistent with previous studies on TPM molecules and other similar systems,[32,34−36] in which the PP decays become faster as the detection wavelength is shifted toward the red. The faster decay rate at the red side of the absorption spectrum was originally ascribed to contamination from the stimulated emission.[32,34] However, the stimulated emission contamination alone cannot explain the sign change of the overall PP signal observed at 620 nm (see Figure 2a). Alternatively, several other authors explained the faster decay as being due to hot ground-state absorption.[35,36] In this work, we will show that the hot ground-state contribution not only produces the wavelength dependence of the PP data but also is responsible for the differences between the PP and homodyne TG signals.

Considering the different nature of the homodyne-detected TG and heterodyne-detected PP, the difference observed in the two measurements is likely to arise from wavelength-dependent contributions of the real component of $P^{(3)}$ to the TG signal, since this component does not contribute to the PP signal. To confirm this hypothesis, heterodyne TG experiments were performed in order to determine both the real and imaginary components of $P^{(3)}$.

III.B. Heterodyne-Detected TG Measurement. OHD-TG measurements for CV in ethanol were also performed at 593 and 620 nm. The phase of the local oscillator was set to be in quadrature or in phase with the signal beam for the measurement of the real and imaginary components of $P^{(3)}$, respectively. The phase was determined by using CS_2, and then the CS_2 sample cell was replaced with an identical cell containing the sample. To remove a small contribution from the homodyne signal, the real and imaginary components were obtained from the difference between two experimental data sets with a π-phase shift in the local oscillator.[26] The accuracy of the phase setting was confirmed as described previously[26] by checking the consistency between the PP and the imaginary components of the TG signals and the consistency between the experimentally measured homodyne TG signal and that reconstructed from the sum of the squared real and imaginary components of $P^{(3)}$ measured by OHD-TG.

From Figure 3, it can be seen that the real and imaginary components are remarkably different at both wavelengths. When excited at the absorption maximum (593 nm), the real and imaginary components are similar to those reported previously for another TPM molecule, malachite green.[26] The flat region between 0.3 and 1.5 ps observed in the imaginary component, which was explained as the induction period[30] in the radiationless decay, is absent in the real component. The real component appears to decay faster than its corresponding imaginary counterpart. The decay profile of the real component at 593 nm appears similar to that of the PP signal and to that of the imaginary component of the TG signal at 620 nm. They all rapidly decay to zero, then change sign, and finally recover back toward zero at later times. Intriguing results were obtained when the system was excited at the red edge of the absorption spectrum (620 nm). The imaginary component is identical to the PP signal as expected, while the real part is negative over the entire time window and a rise is observed in the negative signal, which reaches a minimum at ~1.5 ps. Such a rise in the real component is exactly what we anticipate to account for the difference between the decay profiles of the PP and homodyne TG signals. The difference outlined above between the real and imaginary components is not likely to be due to contamination from the nonresonant solvent contribution, which

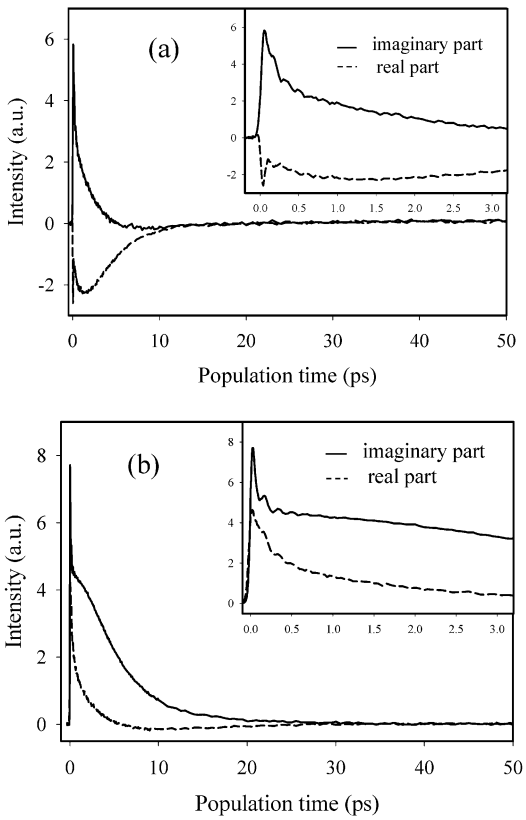

Figure 3. Heterodyne detected TG profiles for crystal violet (CV) in ethanol measured at 620 nm (a) and 593 nm (b).

only influences the third-order signal at short times.[10] It is also unlikely that there is a significant contribution from an acoustic grating because the signal is independent of the sample flow rate. Furthermore, even if an acoustic grating were formed, its oscillation period is typically 10−20 ns and its rise time would be much longer than the current time window.[37]

The wavelength dependence of the amplitudes associated with the real and imaginary components is consistent with the results obtained for a nonreactive system[10] and in accord with the Kramers−Kronig relation.[3,38] According to the Kramers−Kronig relation, the imaginary component (absorption) has the same sign over the entire wavelength range, while the amplitude of the real component (dispersion, n_p) has opposite signs on two sides of the absorption maximum and is zero at a wavelength near the absorption maximum. Although the Kramers−Kronig relation was originally applied to the linear spectrum, a similar relation will also hold between the transient absorption and transient dispersion in the third-order signal.[6,10,39,40] As discussed by Gumy et al.,[39] the real component of $P^{(3)}$ is proportional to $-n_p$, thus it would be negative on the red side of the absorption spectrum and positive on the blue side.[10,37,39] In addition, the wavelength corresponding to the zero amplitude of transient dispersion is usually observed to be located slightly to the red part of the absorption band.[6,10] In the current system, the amplitude associated with the real component at 593 nm, the absorption maximum, is positive rather than zero.

The OHD-TG data were fit to a sum of exponential components, and the fitting parameters are summarized in Table 1. The fits for all four curves require components with both negative and positive amplitudes. The similarity of the time constants associated with different components in each profile suggests that they may not be well resolved from each other. Thus these time constants may not directly represent any physical process. To understand the underlying dynamics, a model for the photophysical process is required. The wavelength dependence of the PP signal was explained as arising from a varying contribution of hot ground-state absorption,[35,36] while the influence of such a contribution on the real component of $P^{(3)}$ and homodyne signal has not been discussed. In the next section we will present a simple model that includes hot ground-state absorption, and a simple calculation based on this model is able to reproduce the major features of the experimental observations.

TABLE 1: Fitting Result for the OHD-TG Measurements at 593 and 620 nm[a]

component	wavelength	A_1	T_1, fs	A_2	T_2, ps	A_3	T_3, ps
real	590 nm	0.63	226	1.54	3.7	1.17	4.6
imaginary	590 nm	0.45	109	0.30	1.0	0.85	4.7
real	620 nm	0.90	21	0.43	1.2	0.53	3.1
imaginary	620 nm	0.59	133	1.00	2.8	0.59	3.9

[a] Data were fit to $A_1 \exp(-t/T_1) + A_2 \exp(-t/T_2) + A_3 \exp(-t/T_3)$.

IV. Discussion

IV.A. Model. All the nonlinear spectroscopic signals can be conveniently calculated by using the response function formalism. The response function for the third-order signal is often calculated with a multi-Brownian oscillator model, which has been presented in detail by Mukamel.[3] The integrated signals in PP,[3] homodyne TG,[3] and OHD-TG[26] are given by

$$\text{PP:} \qquad I(T) \propto \int_{-\infty}^{\infty} dt' \, E_{LO}(t') \, \text{Im} \, P^{(3)}(0, T, t') \tag{1a}$$

$$\text{Homodyne TG:} \qquad I(T) \propto \int_{-\infty}^{\infty} dt' \, |P^{(3)}(0, T, t')|^2 \tag{1b}$$

$$\text{OHD-TG:} \quad I(T) \propto \int_{-\infty}^{\infty} dt' \, E_{LO}(t')[\cos(\phi) \, \text{Im} \, P^{(3)}(0, T, t') + \sin(\phi) \, \text{Re} \, P^{(3)}(0, T, t')] \tag{1c}$$

where $E_{LO}(t)$ is the envelope of the local oscillator electric field, and ϕ is the phase difference between the signal and the LO fields. In the impulsive limit, the third-order polarization $P^{(3)} \propto R$,[3] where the total response function is the sum of contributions from different pathways, $R = \Sigma R_i$, containing the molecular information about the system under study.

The barrierless dynamics in TPM molecules is usually modeled as shown in Figure 1a. The relaxation on the excited state has been successfully described by the model proposed by Bagchi, Fleming, and Oxtoby (BFO).[30] According to the BFO model, the decay on the excited-state surface depends on the shape of the deactivation sink and is usually nonexponential because the population kinetics never reaches steady state. In the case of a broader deactivation sink, the nonexponential behavior is predicted to be less pronounced. The most appropriate microscopic model for the dynamics would be the one where continuous population evolution was connected to the evaluation of the appropriate response functions. An approach similar in spirit was developed to describe energy transfer in incoherent energetically disordered systems by Yang and co-workers.[41,42] However, a parallel treatment for elementary condensed phase chemical dynamics remains to be developed, and we instead use a simpler, intuitive approach, in which different response functions are associated with different regions of the potential energy surface. These response functions are then connected via simple kinetics characterized by exponential decays. Clearly such an approach will not reveal the finer details of the relaxation on either ground or excited-state surfaces, but we expect it to capture the essence of the phenomena involved.

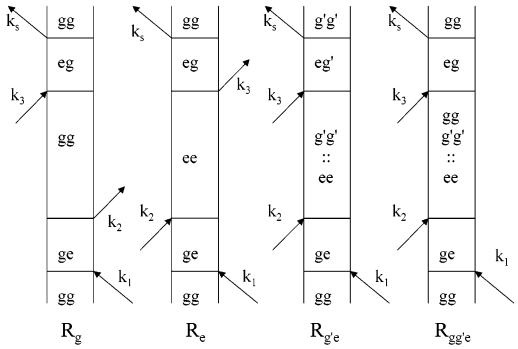

Figure 4. Double-sided Feynman diagrams for the different contributions to the total response function. For simplicity, only the rephasing terms are shown. In each case, a similar diagram can be drawn for the nonrephasing terms. The first two terms represent the contribution from the ground and excited pathways. $R_{g'e}$ represents the contribution from hot ground-state absorption after recovery from the excited state. $R_{gg'e}$ represents the contribution from the decay of the hot ground state to the original ground state. :: in $R_{g'e}$ and $R_{gg'e}$ represent an evolution process from the initially excited state to the hot ground state.

The double-sided Feynman diagrams for these response functions are shown in Figure 4. The original and hot ground state are represented by different states denoted by g and g′. Here only the rephasing term is shown for simplicity. In each case, a similar diagram can be drawn for the nonrephasing terms. For techniques such as transient grating (TG) and pump−probe (PP), where the first two interactions are coincident in time, the rephasing and nonrephasing contributions to the third-order polarization $P^{(3)}$ differ only within the pulse duration and are identical when the population time T is much longer than the pulse duration. Our goal in the present calculation is to obtain the interesting features of our data for population times longer than pulse duration. In this case, for times longer than the dephasing time scale, it suffices to consider only a single set of diagrams, since both rephrasing and nonrephasing sets will give the same result. Four rephasing terms need to be considered to construct the total response function,

$$R = R_g + R_e - R_{g'e} - R_{gg'e} \tag{2}$$

In eq 2, the first two terms correspond to the contributions from the hole on the ground state (R_g) and population on the excited state (R_e). The third term ($R_{g'e}$) corresponds to hot ground state (g′) absorption and the last term ($R_{gg'e}$) corresponds to the hole filling process due to the recovery from the hot ground state. The negative sign of the last two terms arises from the odd number of interactions with the ket and bra sides of the double-sided Feynman diagrams.

Since the deactivation process originates from the excited molecules, R_g contains only the contribution from solvation dynamics, thus $R_g = R_g^0$. Hereafter, the superscript 0 denotes that a separation between solvation dynamics and population kinetics has been made. However, R_e needs to be properly scaled according to the corresponding population kinetics on the excited state. When Markovian population kinetics are assumed, we can write $R_e = R_e^0 e^{-T/\tau_e}$, where τ_e is the time scale on which the molecules in the excited-state move out of the probe laser window.

The hot ground-state contribution also needs to be scaled by the population kinetics,

$$R_{g'e} = R_{g'e}^0 \frac{\tau_c}{\tau_c - \tau_g}(e^{-T/\tau_c} - e^{-T/\tau_g})$$

where τ_g is the rate-determining step from the excited state to the hot ground state and τ_c is the rate of the recovery from the hot ground state to the original ground state. Similarly, the contribution from the recovery process of the hot ground-state $R_{gg'e}$ can be approximated as

$$R_{gg'e} = R_{gg'e}^0\left(1 - \frac{\tau_c}{\tau_c - \tau_g} e^{-T/\tau_c} + \frac{\tau_g}{\tau_c - \tau_g} e^{-T/\tau_g}\right)$$

The total response function is thus given by

$$\begin{aligned} R &= R_g^0 + R_e^0 e^{-T/\tau_e} - R_{gg'e}^0\left(1 - \frac{\tau_c}{\tau_c - \tau_g} e^{-T/\tau_c} + \frac{\tau_g}{\tau_c - \tau_g} e^{-T/\tau_g}\right) - R_{g'e}^0 \frac{\tau_c}{\tau_c - \tau_g}(e^{-T/\tau_c} - e^{-T/\tau_g}) \\ &= R_e^0 e^{-T/\tau_e} + R_g^0\left(\frac{\tau_c}{\tau_c - \tau_g} e^{-T/\tau_c} - \frac{\tau_g}{\tau_c - \tau_g} e^{-T/\tau_g}\right) - R_{g'e}^0 \frac{\tau_c}{\tau_c - \tau_g}(e^{-T/\tau_c} - e^{-T/\tau_g}) \end{aligned} \tag{3}$$

In eq 3, $R_{gg'e}^{'0} = R_g^0$ is assumed by ignoring the history effect.[43] The history effect refers to the effect of the solvation dynamics bringing the molecules back to the ground state at a different position of the solvation coordinate.[43]

Considering the $\pi/2$ phase difference between the polarization and the response function,[3,44] we will continue the discussion in terms of polarization in order to be consistent with the usual convention that the pump−probe signal is proportional to the imaginary component of the third-order polarization. Correspondingly, in the impulsive limit, the total third-order polarization $P^{(3)}$ is

$$P_{tot}^{(3)} = P_e^0 e^{-T/\tau_e} + P_g^0\left(\frac{\tau_c}{\tau_c - \tau_g} e^{-T/\tau_c} - \frac{\tau_g}{\tau_c - \tau_g} e^{-T/\tau_g}\right) - P_{g'e}^0 \frac{\tau_c}{\tau_c - \tau_g}(e^{-T/\tau_c} - e^{-T/\tau_g}) \tag{4}$$

In the case when $\tau_c \gg \tau_g$, i.e., the cooling process is much slower than the nonadiabatic transition to the ground state, eq 4 can be further simplified to

$$P_{tot}^{(3)} \approx P_e^0 e^{-T/\tau_e} + P_g^0 e^{-T/\tau_c} - P_{g'e}^0(e^{-T/\tau_c} - e^{-T/\tau_g}) \tag{5a}$$

$$= P_e^0 e^{-T/\tau_e} + (P_g^0 - P_{g'e}^0)e^{-T/\tau_c} + P_{g'e}^0 e^{-T/\tau_g} \tag{5b}$$

It is worth mentioning that the full phase memory information of the system is contained in the above formulas, which can be calculated by using the full set of diagrams (rephasing and nonrephasing) and including a proper model for the solvation dynamics. In the present study, we only focus our attention on resolving the key features of the population dynamics, thus P_e^0, P_g^0, and $P_{g'e}^0$ are assumed to be constant for simplicity. Note that in the context of above formulas, the signal is defined in terms of transmission intensity, rather than the transient absorption, thus the stimulated emission and ground-state bleaching contribute as positive terms, while excited-state absorption and hot ground-state absorption contribute as negative terms.

IV.B. Model Calculation. A model calculation was made using the formulas outlined above. Equations 4 and 5 each have three exponential components with the same time scales (τ_e, τ_g, and τ_c), the difference between the two equations lies in the

relative amplitudes of the components. Our aim here is to reproduce the qualitative features observed in the various experiments and we will use eq 5 for the sake of convenience and the simplicity of the physical interpretation of the time scales, even though the parameters used in the following calculation do not meet precisely the requirement of this equation. Actually, the same results can also be obtained by using eq 4 with slight adjustment of the relative amplitudes of P^0_e, P^0_g, and $P^0_{g'e}$. Even with exactly the same parameters, similar qualitative features are obtained from both eq 4 and eq 5.

In general, P^0_e, P^0_g, and $P^0_{g'e}$ are all wavelength dependent. P^0_e and P^0_g are usually assumed to be identical at a given wavelength, since they are associated with the same electronic transition (e−g).[9] However, $P^0_{g'e}$ has a different wavelength dependence, since it is associated with the e−g′ transition, which has a different center transition frequency from that of the e−g transition. The fast nonadiabatic transition from the excited state will launch the excited molecules on the ground state vibrationally "hot" with a non-Boltzmann vibrational population distribution. The absorption spectrum of the hot ground state is time-dependent and appears red-shifted and broadened compared to that of the "cold" ground state. It gradually shifts to the blue and narrows and eventually becomes identical to that of the "cold" ground state; i.e., the "hole" on the ground state is completely filled via the cooling process.[36,45,46] This hole-filling process is clearly illustrated by Mataga et al.[46] in their hole-burning study of styryl-8. The authors observed the appearance and evolution of an antihole between the two well-separated holes that correspond to the ground and excited-state contributions, respectively, following the nonadiabatic relaxation from the excited state to the ground state. The antihole corresponds to the contribution of the nonequilibrium hot ground state and has a similar amplitude to the hole associated with the ground-state bleaching. It implies that the hot and the "cold" ground states have similar amplitude at their absorption maxima. In the detailed study of the photodissociation and recombination of iodine by Harris et al.,[45] the absorption spectrum of a nonequilibrated or "hot" ground state prepared by a nonadiabatic transition from a higher electronic excited state was observed to be time dependent, and the absorption maximum shifted from the near-IR toward the normal visible ground-state absorption spectrum as the molecules relaxed. Similar observations of the time-dependent shifting of the "hot" ground-state absorption spectrum were also reported in several other systems.[36,46]

In our simple model, the time-dependent nonequilibrium hot ground state is described by $P_{g'e}$. In the qualitative calculation described here, we assume that the absorption spectrum of $P^0_{g'e}$ peaks at 635 nm, to the red of the equilibrium ground state (see Figure 5a) and its time dependence is described by a single decay arising from the component due to solvation and vibrational dynamics. The ratio of the contributions to the pump probe signal or the imaginary component of $P^{(3)}$ from the hot ground state ($P^0_{g'e}$) and the original ground state (P^0_g), $\mathrm{Im}(P^0_{g'e})/\mathrm{Im}(P^0_g)$ (Figure 5b), can be obtained by the ratio of the two absorption spectra (Figure 5a). The ratio of the real components of $P^{(3)}$, $\mathrm{Re}(P^0_{g'e})/\mathrm{Re}(P^0_g)$ (Figure 5c), can also be obtained from the corresponding transient dispersion spectra. The transient dispersion spectrum for the equilibrium ground state is obtained by first performing a Kramers−Kronig transformation of the corresponding absorption spectrum given in Figure 5a and then multiplying by −1.[10,37,39] The result is further red-shifted to ensure that the zero dispersion wavelength is close to the experimental value, ∼605 nm for the equilibrium ground state (Figure 5a). The transient dispersion spectrum for the hot ground state (Figure 5a) is obtained by applying the same procedure to the corresponding absorption spectrum.

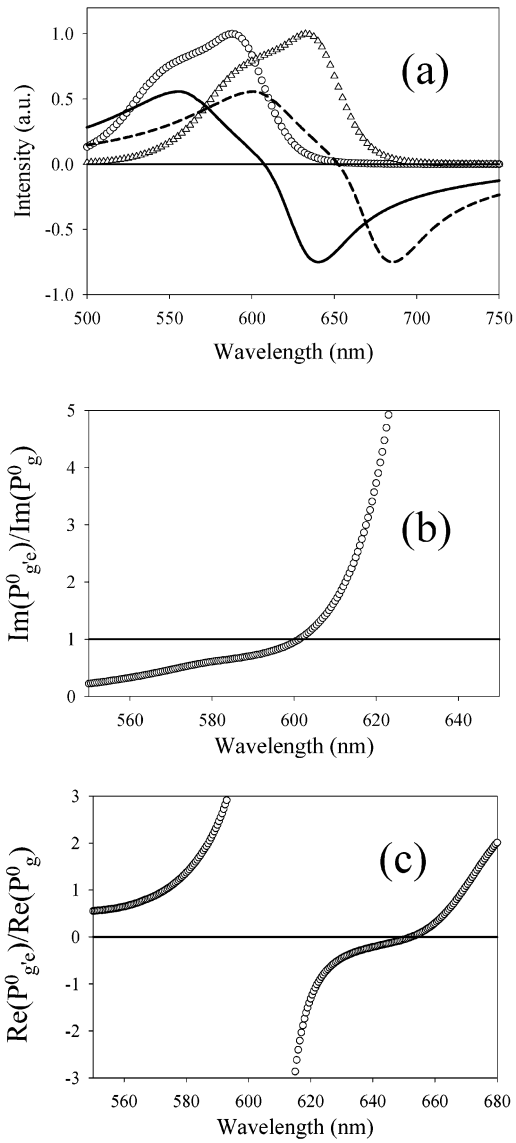

Figure 5. (a) The spectra of the real and imaginary contributions from the relaxed and hot ground states. The spectra of the imaginary components of $P^{(3)}$ (transient absorption) are represented by their linear absorption spectra. The hot ground-state absorption spectrum (open triangles) is obtained by red-shifting the original ground-state absorption spectrum (open circles) by 45 nm to make it peak at ∼635 nm. The spectra of the real components of $P^{(3)}$ (transient dispersion) for the relaxed (solid line) and hot (dashed line) ground states are obtained as described in the text. (b) The wavelength-dependent relative contributions from the hot and relaxed ground states to the imaginary component of $P^{(3)}$ ($\mathrm{Im}(P^0_{g'e})/\mathrm{Im}(P^0_g)$). (c) The wavelength-dependent relative contributions from the hot and relaxed ground states to the real component of $P^{(3)}$ ($\mathrm{Re}(P^0_{g'e})/\mathrm{Re}(P^0_g)$). Note that the wavelength scales are different in each panel.

For the current system at 620 nm, the red edge of the absorption spectrum, the absorption is expected to be stronger for the hot ground state than for the equilibrium ground state due to the red-shifted absorption of the hot ground state.[36,45,46] Therefore, $\mathrm{Im}(P^0_{g'e})$ will be significantly larger than $\mathrm{Im}(P^0_g)$ and the ratio $\mathrm{Im}(P^0_{g'e})/\mathrm{Im}(P^0_g)$ can range from ∼1 to >10 as shown in Figure 5b, assuming a similar maximal amplitude of the hot ground state to that of the "cold" ground state. The exact ratio depends on the position of the detection wavelength with respect to the absorption maxima of the hot and equilibrium ground

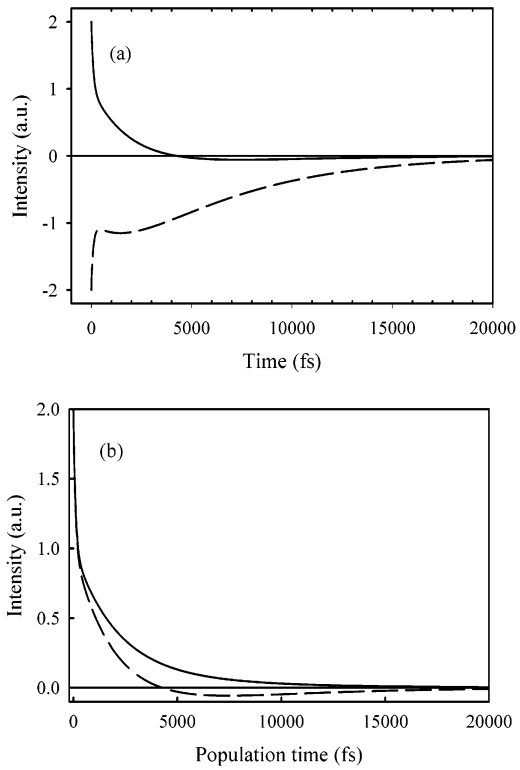

Figure 6. Model calculations for the real (dashed lines) and imaginary (solid lines) components of the third-order polarization at 620 nm (a) and 593 nm (b). As discussed in the text, at 620 nm, the imaginary component is modeled by $y = e^{-T/100} + e^{-T/5500} - 1.35(e^{-T/5500} - e^{-T/2000})$, while the real component is modeled by $y = -e^{-T/100} - e^{-T/5500} - 1.35(e^{-T/5500} - e^{-T/2000})$; at 593 nm, the imaginary component is modeled by $y = e^{-T/100} + e^{-T/5500} - 0.85(e^{-T/5500} - e^{-T/2000})$, while the real component is modeled by $y = e^{-T/100} + e^{-T/5500} - 1.35(e^{-T/5500} - e^{-T/2000})$.

states. When $\mathrm{Im}(P^0_{g'e}) > \mathrm{Im}(P^0_g)$, the amplitude associated with the time constant τ_c will become negative according to eq 5, while the amplitudes associated with τ_e and τ_g are positive, since all P^0_e, P^0_g, and $P^0_{g'e}$ contributions associated with the imaginary components are positive. To illustrate the phenomena underlying the various signals, we have chosen to use amplitudes for the various terms in eq 5 that are consistent with the steady state and expected transient spectra as shown in Figure 5. Within the range of values for the amplitudes that are consistent with our spectral analysis, similar qualitative results are obtained. Thus, the calculated results can be used to illustrate the origin of the different responses observed in the TG and PP signals without focusing on the precise values of the various amplitudes. Using the three time scales chosen to be similar to the fitting parameters, $\tau_e = 100$ fs, $\tau_g = 2000$ fs, and $\tau_c = 5500$ fs, and the relative amplitudes of the three contributions to be $\mathrm{Im}(P^0_e):\mathrm{Im}(P^0_g):\mathrm{Im}(P^0_{g'e}) = 1:1:1.35$, we can reproduce the negative going response and subsequent recovery to zero in the imaginary component of the 620-nm data using eq 5 (Figures 3a and 6a). The features of this imaginary signal can be reproduced as long as $\mathrm{Im}(P^0_{g'e})$ is larger than $\mathrm{Im}(P^0_g)$, and the hole filling process is significantly slower than the nonadiabatic transition rate, i.e., $\tau_c > \tau_g$. A larger $\mathrm{Im}(P^0_{g'e})/\mathrm{Im}(P^0_g)$ value simply results in a larger dip in the negative signal than the one shown in Figure 6a. The situation is different for the real component. 620 nm is located on the red edge of the e−g absorption spectrum, but it can be located at either the blue or the red side of the e−g′ absorption spectrum, depending on the location of the hot ground state absorption maximum. This leads to negative values for the $\mathrm{Re}(P^0_e)$ and $\mathrm{Re}(P^0_g)$ contributions and either a positive or negative value for the $\mathrm{Re}(P^0_{g'e})$ contribution as shown in Figure 5a. From Figure 5b we can see that for the wavelength located between the zero-dispersion wavelength of the original and hot ground states, the ratio $\mathrm{Re}(P^0_{g'e})/\mathrm{Re}(P^0_g)$ is negative (i.e., a positive real component for $P^0_{g'e}$); however, this ratio will become positive when the wavelength is further shifted to the red. Using the same time scales and absolute relative amplitudes as used for modeling the imaginary component at this wavelength, we are able to qualitatively reproduce the experimental data shown in Figure 3a with negative $\mathrm{Re}(P^0_e)$ and $\mathrm{Re}(P^0_g)$ and a positive $\mathrm{Re}(P^0_{g'e})$. The calculated result is shown in Figure 6a, and does a good job of reproducing the rise behavior seen in the negative signal of the real component. In contrast, a choice of negative $\mathrm{Re}(P^0_{g'e})$ results in a remarkably decreased amplitude of the negative signal and thus is strikingly different from the experimental profile. The ability to reproduce the experimental data with the selected amplitudes indicates that the sign difference between $\mathrm{Re}(P^0_g)$ and $\mathrm{Re}(P^0_{g'e})$, rather than the absolute magnitude of $\mathrm{Re}(P^0_g)/\mathrm{Re}(P^0_{g'e})$, is responsible for the features observed in the real component at 620 nm. It also implies that the hot ground-state absorption peaks at a wavelength longer than 620 nm so as to give a positive real component of $P^0_{g'e}$. Although the absolute value of the $\mathrm{Re}(P^0_g)/\mathrm{Re}(P^0_{g'e})$ ratio was taken to be identical in the calculations outlined above, typically we expect the magnitude of $\mathrm{Re}(P^0_g)/\mathrm{Re}(P^0_{g'e})$ and $\mathrm{Im}(P^0_g)/\mathrm{Im}(P^0_{g'e})$ will be different at a given wavelength.

The situation is different at 593 nm, which is located on the blue side of zero-dispersion wavelength of the e−g and e−g′ spectra as manifested by the positive-signed real component shown in Figures 3b and 5a. Thus, all the contributions from P^0_e, P^0_g, and $P^0_{eg'}$ are positive in the real and imaginary components. The dispersion spectrum is usually much broader than the corresponding absorption spectrum (see cf. Figure 5a), and this leads to a larger ratio between the real and the imaginary components as the wavelength is detuned farther away from the zero-dispersion wavelength. Therefore, it is reasonable to assume that the ratio between the real and imaginary components for the hot ground state is larger than that for equilibrium ground state at 593 nm, i.e., $\mathrm{Re}(P^0_{g'e})/\mathrm{Im}(P^0_{g'e}) > \mathrm{Re}(P^0_g)\mathrm{Im}(P^0_g)$ (which leads to $\mathrm{Re}(P^0_{g'e})/\mathrm{Re}(P^0_g) > \mathrm{Im}(P^0_{g'e})/\mathrm{Im}(P^0_g)$), owing to the red-shifted absorption maximum of the hot ground state[36,45,46] and the correspondingly shifted zero-dispersion wavelength. Choosing $\mathrm{Im}(P^0_e):\mathrm{Im}(P^0_g):\mathrm{Im}(P^0_{g'e}) = 1:1:0.85$ and $\mathrm{Re}(P^0_e):\mathrm{Re}(P^0_g):\mathrm{Re}(P^0_{g'e}) = 1:1:1.35$ and using identical time scales for both enable us to reproduce the different decay profiles in the real and imaginary components observed experimentally at 593 nm (see Figures 3b and 6b). From Figure 6b,c, we can see that this choice of the relative magnitudes of P^0_g and $P^0_{g'e}$ is reasonable, as 593 nm is at the absorption maximum and thus P^0_g will have a larger contribution than $P^0_{g'e}$ to the imaginary component. Furthermore, we note that a range of smaller $P^0_{g'e}$ contributions is capable of producing similar qualitative features. In contrast, from Figure 5a, we see the dispersion contribution at 593 nm is smaller than that on the blue side. The red-shifted absorption and zero-dispersion wavelength of the hot ground state place this detection wavelength (593 nm) on the blue side of the e−g′ transition. This may result in a smaller contribution from P^0_g than from $P^0_{g'e}$ in the real component at this wavelength.

The calculations above show that the different ratios of $P^0_{g'e}/P^0_g$ in the real and imaginary components are the key factor

in reproducing the different kinetics associated with the real and imaginary components of the total $P^{(3)}$. Moreover, as the detection wavelength is further shifted to the blue, the ratio $\mathrm{Re}(P^0_{g'e})/\mathrm{Re}(P^0_g)$ will decrease and become less than 1 (cf. Figure 5c). This will then result in a real component with no negative component (amplitudes associated with τ_e, τ_g, and τ_c are all positive, cf. eq 5), giving a decay profile similar to that of the imaginary component at 593 nm as shown in Figures 3b and 6b. Such behavior was indeed observed in our experiment (data not shown). Considering the fact that the excited state absorption is usually observed on the blue side of the ground-state absorption spectrum[31] in this molecule, which would further complicate the analysis, we limit our analysis to the qualitative level for the spectral region given above.

In a previous paper,[26] we reported an OHD-TG measurement for malachite green in ethanol carried out at an excitation wavelength corresponding to the absorption maximum. A dominant component with similar time scales was observed in both the real and imaginary components of the third-order signal. In addition, a minor and slower component was observed in both components of the third-order signal with similar time scales but oppositely signed amplitudes. The physical meaning of these results can be understood rather straightforwardly in the context of our present model in terms of eq 5. The dominant component corresponds to the rate of the ground-state recovery and the slower component is associated with the cooling process in the hot ground state. It is clear that the amplitude of the cooling process could be either positive or negative, depending on the relative amplitude of P^0_e and $P^0_{g'e}$ in the two components.

It has to be admitted that the model outlined is a very crude one. First, important processes have not been taken into account in this model, such as the intramolecular vibrational relaxation and energy redistribution on the electronic excited state. Second, the solvation contribution to the stimulated emission (P^0_e) and ground-state bleaching (P^0_g) is assumed to be identical in both the real and imaginary components (the relative amplitude of P^0_g and P^0_e will only affect the amplitude of the initial spike and will not change the qualitative features of the model calculation). The stimulated emission is assumed to decay rapidly out of the laser window in the current one-color experiment, since the excitation and probe wavelengths are located outside of the fluorescence spectrum. Third, the absorption spectrum of $P^0_{g'e}$ was approximated by a red-shifted spectrum of the equilibrium ground state and no change of spectral width was considered. A more quantitative calculation will require incorporating a detailed description of this time dependence of the spectral narrowing and blue shifting. Finally, the induction period effect, a major feature in barrierless large-amplitude motion to a "sink" region of the potential energy surface, is also not considered in this model. Given the crudeness of the present model, we did not attempt a quantitative interpretation of the data for the TPM molecules but rather concentrated on a qualitative interpretation of the striking features observed in these molecules. Our simple model successfully explains the differences in the real and imaginary components and their wavelength-dependent behaviors observed in the experiments. The different decay profiles in the real and imaginary components at two wavelengths can be qualitatively reproduced by a single formula with identical time constants and wavelength-dependent amplitudes. The relative amplitudes of the different contributions are chosen to be consistent with a simple model for the spectral evolution. The fact that those parameters are able to qualitatively reproduce the major features observed experimentally, on the other hand, suggests that extending the analysis to include detailed description of time-resolved spectra would yield an accurate description of the dynamics.

IV.C. Further Implications. The real and imaginary components of the third-order polarization of crystal violet in ethanol solution were found to be distinctly different. We believe that this arises from different contributions to the two responses from the hot ground state, with respect to the contributions from stimulated emission and ground-state bleaching. In general, in a multilevel system, the different terms associated with different electronic transitions are expected to contribute with different signs and amplitudes to the real and imaginary components of $P^{(3)}$ at a specific wavelength. Since the homodyne signal is a sum of squared real and imaginary components with different decay profiles, the parameters obtained from the direct fitting of the homodyne signal may not be physically meaningful, at least in a straightforward manner. In general, care should be taken in the characterization of the homodyne measurements on complex multilevel systems. Similar considerations will also apply, in principle, to photon echo experiments, but we have not considered this aspect in any detail so far.

V. Summary

In this paper, we reported a heterodyne transient grating measurement of crystal violet in ethanol, in which a fast decay to the ground state occurs after photoexcitation. The real and imaginary components were found to be strikingly different and strongly wavelength dependent in this system. Such a difference has not been noted previously, and it is responsible for the different decay features in the PP and homodyne TG signals. A model incorporating hot ground-state absorption was proposed and analyzed based on the appropriate double-sided Feynman diagrams. Calculations based on this simple model are able to successfully reproduce the major features observed in the experiments. The relaxation process after photoexcitation in the TPM molecules can be described by the nonadiabatic transition followed by a slower cooling process. The striking difference between the decay profiles of the real and imaginary components and their wavelength dependence are mainly due to the wavelength-dependent amplitudes of the various contributions to the signal, rather than to changes of the corresponding time constants or the contribution of new components at particular wavelengths. We believe that the qualitative model described here will provide a firm basis for quantitative modeling based on realistic potential energy surfaces.

Acknowledgment. This work was supported by a grant from National Science Foundation. We thank Drs. Mino Yang and Laura Kaufman for comments on the manuscript.

References and Notes

(1) Fleming, G. R. *Chemical applications of ultrafast spectroscopy*; Oxford University Press: New York, 1986.
(2) Rullière, C. *Femtosecond laser pulses: principles and experiments*; Springer: Berlin; New York, 1998.
(3) Mukamel, S. *Principles of nonlinear optical spectroscopy*; Oxford University Press: New York, 1995.
(4) Eichler, H. J.; Günter, P.; Pohl, D. W. *Laser-induced dynamic gratings*; Springer-Verlag: Berlin, New York, 1986.
(5) Fayer, M. D. *Annu. Rev. Phys. Chem.* **1982**, *33*, 63.
(6) Högemann, C.; Pauchard, M.; Vauthey, E. *Rev. Sci. Instrum.* **1996**, *67*, 3449.
(7) Fourkas, J. T.; Fayer, M. D. *Acc. Chem. Res.* **1992**, *25*, 227.
(8) Myers, A. B.; Hochstrasser, R. M. *IEEE J. Quantum Electron.* **1986**, *22*, 1482.
(9) Joo, T. H.; Jia, Y. W.; Yu, J. Y.; Lang, M. J.; Fleming, G. R. *J. Chem. Phys.* **1996**, *104*, 6089.
(10) Xu, Q.-H.; Ma, Y.-Z.; Stiopkin, I. V.; Fleming, G. R. *J. Chem. Phys.* **2002**, *116*, 9333.

(11) Owyoung, A. *IEEE J. Quantum Electron.* **1978**, *14*, 192.
(12) Eesley, G. L.; Levenson, M. D.; Tolles, W. M. *IEEE J. Quantum Electron.* **1978**, *14*, 45.
(13) Lotshaw, W. T.; McMorrow, D.; Thantu, N.; Melinger, J. S.; Kitchenham, R. *J. Raman. Spectrosc.* **1995**, *26*, 571.
(14) Waldeck, D.; Cross, A. J., Jr.; McDonald, D. B.; Fleming, G. R. *J. Chem. Phys.* **1981**, *74*, 3381.
(15) Xu, Q.-H.; Fleming, G. R. *J. Phys. Chem. A* **2001**, *105*, 10187.
(16) Xu, Q.-H.; Fleming, G. R. Unpublished results.
(17) Scherer, N. F.; Matro, A.; Ziegler, L. D.; Du, M.; Carlson, R. J.; Cina, J. A.; Fleming, G. R. *J. Chem. Phys.* **1992**, *96*, 4180.
(18) Chang, Y. J.; Cong, P.; Simon, J. D. *J. Phys. Chem.* **1995**, *99*, 7857.
(19) Matsuo, S.; Tahara, T. *Chem. Phys. Lett.* **1997**, *264*, 636.
(20) Goodno, G. D.; Dadusc, G.; Miller, R. J. D. *J. Opt. Soc. Am. B* **1998**, *15*, 1791.
(21) Goodno, G. D.; Astinov, V.; Miller, R. J. D. *J. Phys. Chem. A* **1999**, *103*, 10 630.
(22) Goodno, G. D.; Astinov, V.; Miller, R. J. D. *J. Phys. Chem. B* **1999**, *103*, 603.
(23) Goodno, G. D.; Miller, R. J. D. *J. Phys. Chem. A* **1999**, *103*, 10 619.
(24) Maznev, A. A.; Nelson, K. A.; Rogers, T. A. *Opt. Lett.* **1998**, *23*, 1319.
(25) Khalil, M.; Demirdoven, N.; Golonzka, O.; Fecko, C. J.; Tokmakoff, A. *J. Phys. Chem. A* **2000**, *104*, 5711.
(26) Xu, Q.-H.; Ma, Y.-Z.; Fleming, G. R. *Chem. Phys. Lett.* **2001**, *338*, 254.
(27) Lewis, G. N.; Magal, T. T.; Lipkin, D. *J. Am. Chem. Soc.* **1942**, *64*, 1774.
(28) Förster, T.; Hoffman, G. *Z. Phys. Chem., Neue Folge (West Germany)* **1971**, *75*, 63.
(29) Oster, G.; Nishijima, Y. *J. Am. Chem. Soc.* **1956**, *78*, 1581.
(30) Bagchi, B.; Fleming, G. R.; Oxtoby, D. W. *J. Chem. Phys.* **1983**, *78*, 7375.
(31) Duxbury, D. F. *Chem. Rev.* **1993**, *93*, 381.
(32) Ben-Amotz, D.; Harris, C. B. *J. Chem. Phys.* **1987**, *86*, 4856.
(33) Xu, Q. H.; Scholes, G. D.; Yang, M.; Fleming, G. R. *J. Phys. Chem. A* **1999**, *103*, 10348.
(34) Åberg, U.; Sundström, V. *Chem. Phys. Lett.* **1991**, *185*, 461.
(35) Walker, G. C.; Åkesson, E.; Johnson, A. E.; Levinger, N. E.; Barbara, P. F. *J. Phys. Chem.* **1992**, *96*, 3728.
(36) Kovalenko, S. A.; Schanz, R.; Farztdinov, V. M.; Hennig, H.; Ernsting, N. P. *Chem. Phys. Lett.* **2000**, *323*, 312.
(37) Högemann, C.; Vauthey, E. *Isr. J. Chem.* **1998**, *38*, 181.
(38) Loudon, R. *The quantum theory of light*, 2nd ed.; Clarendon Press: Oxford, 1983.
(39) Gumy, J. C.; Nicolet, O.; Vauthey, E. *J. Phys. Chem. A* **1999**, *103*, 10737.
(40) de Boeij, W. P.; Pshenichnikov, M. S.; Wiersma, D. A. *Chem. Phys.* **1998**, *233*, 287.
(41) Agarwal, R.; Yang, M.; Xu, Q. H.; Fleming, G. R. *J. Phys. Chem. B* **2001**, *105*, 1887.
(42) Yang, M.; Fleming, G. R. *J. Chem. Phys.* **2000**, *113*, 2823.
(43) Yang, M.; Ohta, K.; Fleming, G. R. *J. Chem. Phys.* **1999**, *110*, 10243.
(44) Gallagher Faeder, S. M.; Jonas, D. M. *Phys. Rev. A* **1998**, *62*, 033820.
(45) Harris, A. L.; Berg, M.; Harris, C. B. *J. Chem. Phys.* **1986**, *84*, 788.
(46) Murakami, H.; Kinoshita, S.; Hirata, Y.; Okada, T.; Mataga, N. *J. Chem. Phys.* **1992**, *97*, 7881.